NOBLE METAL MASS TRANSPORT MODEL FOR MOLTEN SALT REACTOR ANALYSIS IN VERA-CS

Samuel A. Walker[1], Zack Taylor[2], Robert Salko[3], Benjamin Collins[3], and Wei Ji[1]

[1]Rensselaer Polytechnic Institute
110 8th Street, Troy, NY 12180, USA

[2]University Of Tennessee
Circle Park Drive, Knoxville, TN 37996, USA

[3]Oak Ridge National Laboratory
1 Bethel Valley Road, Oak Ridge, TN 37830, USA

walkes4@rpi.edu, rtaylo45@vols.utk.edu, salkork@ornl.gov, collinsbs@ornl.gov, jiw2@rpi.edu

ABSTRACT

Molten salt reactor (MSR) designs require robust multiphysics modelling capabilities to further the development of this next generation technology. Due to the unique liquid fuel design, traditional reactor physics analysis codes do not capture all of the important physics of these reactors. This work builds upon a general species transport model implemented into the multiphysics core simulator suite VERA-CS, by adding source and sink models for insoluble fission products, specifically the noble metals. Noble metal (NM) fission products are born in the fuel-salt, but do not form stable fluorides, and instead plate-out on various surfaces in the reactor fuel loop. A concentration gradient advection-diffusion based mass transfer model is implemented into the general species transport model within CTF – the subchannel thermal hydraulics code in VERA-CS – and verified using convergence tests in space and time. Two noble metal decay chains are analyzed, and their steady state bulk liquid densities and surface concentrations are calculated for a simple flow loop in CTF that is roughly representative of the Oak Ridge National Laboratory Molten Salt Reactor Experiment (MSRE) [1]. Insoluble species ^{99}Mo decaying to ^{99}Tc captures wall accumulation of decaying species, and insoluble ^{131}Sb to semi-soluble ^{131}Te to soluble ^{131}I captures wall loss of decaying species. Results are compared with MSRE data and the possible multiphysics effects of this phenomena are identified. Future work to enhance the robustness of the physical model and couple it with neutronics to evaluate the effects of NM mass transport is discussed.

KEYWORDS: MASS TRANSPORT, MOLTEN SALT REACTOR, VERA-CS, CTF

1. INTRODUCTION

Due to the surge of commercial interest in molten salt reactors (MSRs) in the United States and abroad, robust multiphysics modelling capabilities are needed to further develop this distinctive reactor type. The first comprehensive demonstration of this technology was the Molten Salt Reactor Experiment (MSRE), which ran during the 1960s at Oak Ridge National Laboratory (ORNL) [1]. The MSRE used a liquid fuel form mixed with a molten coolant salt; this fuel sets the MSRE apart from traditional solid fuel reactors.

1.1. Spatial and Time Dependent Fuel Salt Composition

One key challenge is the need to track the spatial and time dependent fuel salt composition as it cycles through the reactor core, pump, and heat exchanger. While typical reactor analyses assume stationary fuel and fission products (FPs) in the core, MSRs have liquid fuel which is advected throughout the primary loop or integral design. In a traditional solid fueled reactor, there is a time dependence of the fuel composition as it experiences burnup, whereas in the case of MSRs with the advection of the fuel and FPs, there is an additional spatial dependence of the fuel salt composition as it cycles through the loop.

This spatial dependence is especially important for insoluble FPs which do not form stable fluorides with the carrier salt. Noble gases (NGs) and noble metal (NM) FPs are insoluble in the fuel salt during normal reactor operation and precipitate out, eventually leaving the fuel salt stream through some sort of mass transfer mechanism. These volatile FPs will ultimately deposit or accumulate somewhere in the reactor's primary loop unless some sort of filter, or extraction mechanism is implemented into the loop.

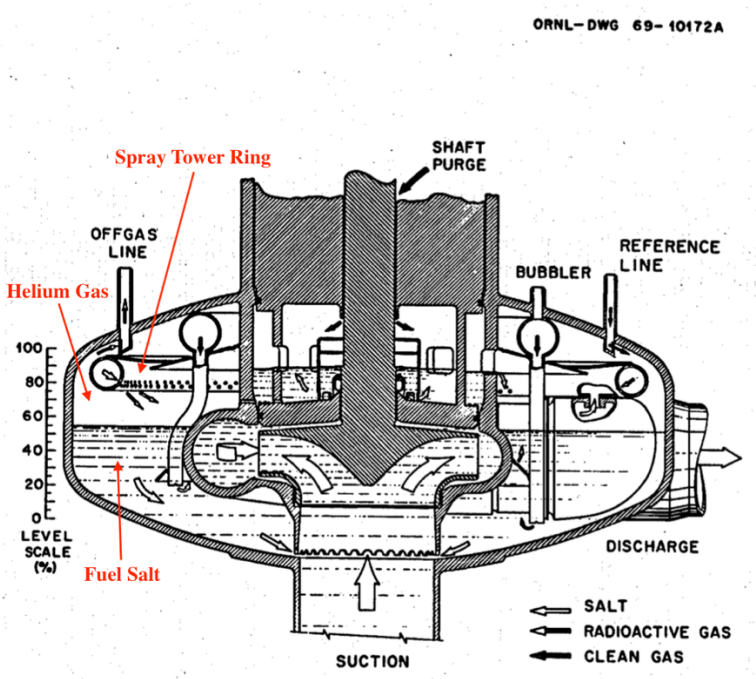

Figure 1. MSRE Pump Bowl Schematic [2].

During the MSRE, NG FPs were constantly extracted through a spray tower liquid-gas contactor located in pump bowl seen above in Figure 1. The primary purpose of this design was to extract the ^{135}Xe from the reactor due to its large thermal neutron absorption cross section thereby minimizing its effect as a neutron poison. Additionally, the free liquid-gas interface in the pump bowl allowed for thermal fuel-salt expansion and theoretically would keep the reactor single-phase by extracting the NGs via the helium cover gas into an off-gas system before the NGs coalesced into substantial sized bubbles capable of altering the flow field. It is important to note that the impinging fuel salt jets from the spray tower created a significant amount of turbulence and churning along with the temporary entrainment of helium gas, which resulted in a frothy well mixed fluid inside the pump bowl [2].

40	41	42	43	44	45	46	47	48	49	50	51	52
Zr	**Nb**	**Mo**	**Tc**	**Ru**	**Rh**	**Pd**	**Ag**	**Cd**	**In**	**Sn**	**Sb**	**Te**
Zirconium	Niobium	Molybdenur	Technetium	Ruthenium	Rhodium	Palladium	Silver	Cadmium	Indium	Tin	Antimony	Tellurium
91.224	92.906	95.95	(98)	101.07	102.91	106.42	107.87	112.41	114.82	118.71	121.76	127.60

Figure 2. Noble Metal Fission Products.

NM FPs on the other hand, here shown in Figure 2 above, formed metallic nano and micro particles which were unwetted by the fuel salt and eventually deposited onto surfaces in the primary loop in order to escape the fuel salt. One of these surfaces included the liquid-gas interface that existed in the pump bowl seen in Figure 1. The turbulent churning environment with the entrained helium bubbles during the ^{233}U runs drastically increased the amount of NM deposition in the pump bowl. ^{235}U runs on the other hand had very little helium entrainment, and as a result the majority of NMs deposited on the largest surface area region in the loop which is the heat exchanger [3].

1.2. Importance of Noble Metal Deposition

In addition to the impact NM mass transfer will have on the evolving fuel salt composition, NM plate-out will create a decay heat source that may be found outside of the core. In the case of a large power reactor, this hot spot generation may create a significant amount of heat that could affect the thermal-hydraulics of the reactor or could even lead to damage. If the localized decay heat source is found in the heat exchanger, this may not be of great concern during normal operation but could be a large issue in the case of a loss of coolant accident. Additionally, the fouling of the heat exchanger through NM deposition could change the heat transfer coefficient or could even create clogs in the tubes, depending on the design [4]. Lastly, it was noted during the ^{233}U MSRE runs that a large majority of NMs deposited on the liquid-gas interface that exists in the pump-bowl shown in Figure 1 due to helium bubble entrainment and NM deposition and transport via the bubbles [3]. Beyond creating a significant amount of decay heat in the pump-bowl, it is unclear what sort of effects NM deposition will have on pump performance.

2. METHODOLOGY

In a previous work, a general species transport model was implemented into CTF, which is the thermal hydraulics subchannel code within VERA-CS [5]. The general mass transport model was implemented into CTF so that any number of interdependent species can be tracked in the system; however, the user must define the species, as well as their source terms, dependencies, and boundary conditions.

This current work extends this general species transport model to include sink/source terms and dependencies specific for tracking insoluble NM FPs. Since NMs exit the bulk fluid flow via diffusion/advection, these species require special tracking capabilities so that the resulting fuel-salt composition, and decay heat generation can be correctly determined in light of NM mass transfer. Accordingly, a concentration gradient advection-diffusion based mass transfer model is incorporated into the general species transport model within CTF so that these insoluble NM species can be mechanistically tracked throughout the reactor primary loop.

The FP decay chains ^{99}Mo – ^{99}Tc and ^{131}Sb – ^{131}Te – ^{131}I are used to demonstrate the unique species transport problem that exists in MSRs which this work seeks to elucidate, where the color red indicates an insoluble NM, the color orange indicates a semi-soluble species (some forming fluorides and some existing in gaseous or metallic form), and the color green indicates a soluble fluoride [1]. In this way, it is important to track the evolving species as they change from insoluble to soluble and back again since they will behave differently in the fuel salt along each step of the decay chain.

2.1. Isotopic Species Tracking with Phase Associated Transport

Species born in the fuel salt are assumed to be uniformly dispersed as nano-particles (NMs), nano-bubbles (NGs), or stable fluorides with the fuel salt. In all of these cases, the species born in the fuel salt from fission and decay are associated with the liquid fuel-salt denoted by a (l) phase indicator, which specifies how these species are being transported – directly with the bulk velocity field of the liquid fuel salt.

In the case of the NMs which deposit onto surfaces in the reactor, these species are denoted by a (*s*) phase indicator since they have left the fuel salt stream and have become immobile on the wall. This sticking action on the wall is due to van der Waals adhesion forces, but some NMs can form an oxide layer on the Hastelloy N structural material or possibly a carbide with the graphite moderator in the core [1][4]. These (*s*) species are not transported, but simply accumulate and decay in the region where they were deposited.

In light of this convention, it is important to note here that ^{99}Mo – ^{99}Tc are both insoluble NMs which demonstrates the cumulative deposition of solid NM species plating out on the surfaces that exist in the channel, where ^{99}Mo – ^{99}Tc is expanded into four total species ^{99}Mo(*l*) - ^{99}Mo(*s*) - ^{99}Tc(*l*) - ^{99}Tc(*s*). In contrast, the ^{131}Sb – ^{131}Te – ^{131}I decay chain showcases the insoluble ^{131}Sb NM decaying to a sometimes-soluble fluoride, sometimes insoluble gas ^{131}Te, which then finally decays into a soluble ^{131}I fluoride. This decay chain is expanded into four total species ^{131}Sb(*l*) - ^{131}Sb(*s*) - ^{131}Te(*l*) - ^{131}I(*l*) that show the temporary deposition of NMs onto the wall and then their role as a source to soluble species later on which are then transported by the liquid fuel (*l*).

2.2. Concentration Gradient Diffusion NM Mass Transfer Model

The mass transfer model implemented into CTF for NM deposition is a simple solid-liquid interface or thin film model in which a mass transfer coefficient captures the combined result of both advection and diffusion, and the mass transfer is driven by a concentration gradient across the thin film interface [6].

$$S_{deposition} = \frac{KA_{surf}}{V_{cell}}\left(\rho_{bulk} - \rho_{interface}\right) \quad (1)$$

Starting from the left-hand side in Eq. (1), the terms include source term change in mass density with respect to time, the mass transfer coefficient K multiplied by the surface area available for deposition divided by the control volume multiplied by the difference in the mass density in the bulk control volume and the equilibrium mass density that exists in the liquid at the solid-liquid interface or deposition surface.

2.2.1 Assumptions

To implement this model, some assumptions have been made in lieu of the required material properties and experimental data. One such assumption is the concentration of the species in the liquid at the interface, $\rho_{\text{Interface}}$, which is the concentration that is soluble in the fuel salt and has formed stable ionic bonds with the fluoride. For simplicity and based on MSRE experience, the solubility, and therefore the species concentration in the liquid at the surface interface, will be set to zero [3]. Therefore, every NM atom will eventually leave the fuel salt where it is born and deposit onto a surface, since the surface is acting as an infinite sink. Ultimately this means that if NM generation ceases, every NM will be found on a surface since the NMs do not form fluorides with the salt and therefore none will remain in the liquid in either the bulk flow or at the interface. This is obviously not the case, since there will be a small equilibrium amount of NMs which do form fluorides in the salt, but this amount should be negligible if the redox potential of the fuel-salt is correctly controlled [3].

The mass transfer coefficients K also require certain assumptions. As a proof of concept, the mass transfer coefficients used in this work are taken directly from MSRE data, in which the Dittus-Boelter correlation for turbulent flows, and other mass transfer correlations using the corresponding geometry and flow conditions are used to determine mass transfer coefficients for four primary loop regions assuming a uniform diffusion coefficient for all NMs [3]. Current work is incorporating updated mass transfer correlations and using the geometry, temperature distribution, and flow conditions calculated by CTF to determine the correct mass transfer coefficients for each region in the primary loop.

Lastly, the strength of the adhesion of NMs on the surfaces in the reactor is not currently taken into account. Some NMs will form ionic bonds with the graphite in the moderator, but the majority of NMs form colloidal agglomerates with one another and are held on to surfaces through bulk van der Waals adhesion forces between the NMs and the surfaces [4]. It is assumed that once the NMs have attached to a surface, they stay their indefinitely, which may not be the case due to changes in temperature, redox potential, and flow field. Also, if a NM decays into a soluble species, it is assumed that there is no resistance for it to 'recoil' away from the surface and rejoin the bulk flow, which may not be the case. These micro-level processes may play important roles for certain species (like Te, I, and Nb) in determining their behavior at the solid-liquid and liquid-gas interface [1].

2.3. Transport Equations

The governing differential equation for species transport in CTF is shown in Eq. (2) below.

$$\frac{\partial \rho_{s(p)}}{\partial t} = -\nabla \cdot \left(\rho_{s(p)} v\right) + S \tag{2}$$

Starting from the left-hand side in Eq. (2), the terms include change in the mass density of a certain species (subscript s) and phase (p) with respect to time, advective mass transport due to a velocity field, and finally, any source or sink terms of which Eq. (1) shown earlier is just one type of sink/source. We then apply Eq. (2) to the FP decay chain of ^{99}Mo – ^{99}Tc to yield Eqs. (3), (4), (5), and (6) which characterize the species traveling through a MSR core channel.

$$\frac{\partial \rho_{Mo(l)}}{\partial t} = -\nabla \cdot \left(\rho_{Mo(l)} v\right) + \frac{M_{Mo}}{N_A} \gamma_{Mo} \Sigma_f \phi - \lambda_{Mo} \rho_{Mo(l)} - \sigma_{a,Mo} \phi \rho_{Mo(l)} - \frac{KA_{surf}}{V_{cell}} \rho_{Mo(l)} \tag{3}$$

$$\frac{\partial \rho_{Mo(s)}}{\partial t} = \frac{KA_{surf}}{V_{cell}} \rho_{Mo(l)} - \lambda_{Mo} \rho_{Mo(s)} - \sigma_{a,Mo} \phi \rho_{Mo(s)} \tag{4}$$

$$\frac{\partial \rho_{Tc(l)}}{\partial t} = -\nabla \cdot \left(\rho_{Tc(l)} v\right) + \frac{M_{Tc}}{N_A} \gamma_{Tc} \Sigma_f \phi + \frac{M_{Tc}}{M_{Mo}} \lambda_{Mo} \rho_{Mo(l)} - \lambda_{Tc} \rho_{Tc(l)} - \sigma_{a,Tc} \phi \rho_{Tc(l)} - \frac{KA_{surf}}{V_{cell}} \rho_{Tc(l)} \tag{5}$$

$$\frac{\partial \rho_{Tc(s)}}{\partial t} = \frac{KA_{surf}}{V_{cell}} \rho_{Tc(l)} + \lambda_{Mo} \rho_{Mo(s)} - \lambda_{Tc} \rho_{Tc(s)} - \sigma_{a,Tc} \phi \rho_{Tc(s)} \tag{6}$$

As can be seen above, the two isotopes are divided into four equations to allow for the explicit tracking of species advected by bulk fluid flow and denoted by (l), and those species which have exited the flow and have become stationary after depositing onto a surface as denoted by (s).

The source term for ^{99}Mo(l), the species present in the flow, is production from fission, and sink terms include decay to ^{99}Tc(l), transmutation, and deposition to ^{99}Mo(s). The source term for ^{99}Mo(s), the species present on the channel wall/surface, is deposition from ^{99}Mo(l), and the sink terms include decay to ^{99}Tc(l), and transmutation. The source terms for ^{99}Tc(l), include production from fission and decay of ^{99}Mo(l), and sink terms include decay, transmutation, and deposition to ^{99}Tc(s). Lastly, the source terms for ^{99}Tc(s), include deposition from ^{99}Tc(l), and decay from ^{99}Mo(s), and sink terms include decay and transmutation.

Similar transport equations can be derived for the ^{131}Sb – ^{131}Te – ^{131}I decay chain with the exception that ^{131}Te(l) has two source terms from the decay of both ^{131}Sb(l) and ^{131}Sb(s). Last thing to note is that all species generated directly from fission are born in the liquid and are initially transported by the (l) phase.

3. RESULTS

3.1. Verification of NM Mass Transfer Deposition Model

Various verification tests were run to ensure the NM mass transfer model was correctly implemented into CTF. Since we are tracking isotopic species and differentiating between their possible phases that they may be associated with (eg. ^{99}Mo(g), ^{99}Mo(l), ^{99}Mo(s)) it is important that the coupling between these species is implemented correctly.

Seen below in Figure 3, a no flow test was run to model the ^{131}Sb – ^{131}Te – ^{131}I decay chain sitting in a tank to ensure the source coupling between all of the species is correct. The equations implemented for this test are similar to Eqs. (3)-(6) only without the advection term since the velocity is set to zero. The time steps are refined from 10,000s to 10s, and we see a good 1st order convergence in the absolute error of the computed solution against the analytical solution as the species close in on their steady-state values.

In Figure 4 below, a single channel axial advection test is run for the ^{99}Mo – ^{99}Tc decay chain represented by Eqs. (3)-(6). The steady state results of the mass densities along the MSR core channel are compared with the analytical solution and we see 1st order convergence in space as we refine the space step from dx = 5e-2 ft to dx = 6.25e-3 ft, with very low absolute errors. Overall, the model and the general species solver behave as expected.

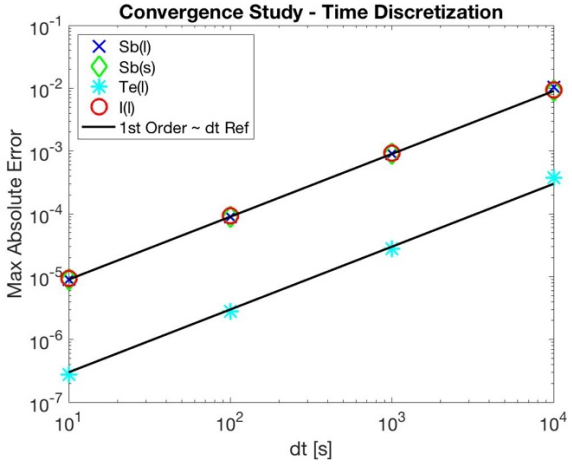

Figure 3. Time Discretization Convergence.

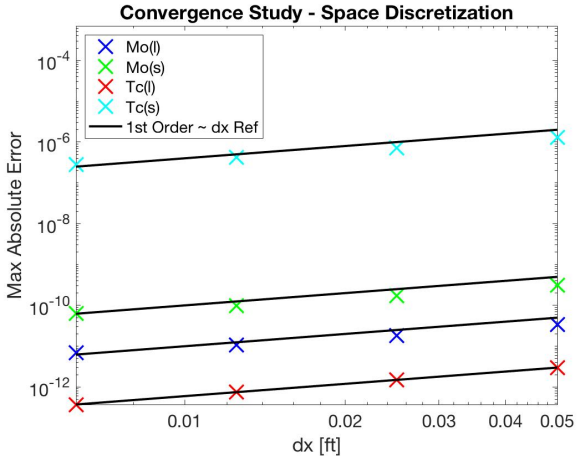

Figure 4. Space Discretization Convergence.

3.2. Simple MSRE Loop Analysis

A simplified MSRE loop geometry was used to illustrate NM behavior in the MSRE in accordance with the advection-diffusion driven mass transfer model implemented in this work [5]. This geometric model was previously designed primarily to ensure accurate velocities in the core. Corrected volumes and cumulative surface areas for four main regions in the MSRE primary loop were superimposed on this rudimentary MSRE loop geometry in hopes of capturing the general NM deposition pattern seen in the MSRE [3].

The steady state solutions for the bulk fluid mass densities and mass surface concentrations for the ^{99}Mo – ^{99}Tc decay chain in the MSRE Simple Loop are presented below in Figures 5 – 8. Looking first at the bulk liquid species Mo(l) in Figure 5, the mass density increases in the core due to generation from fission, and the 's' curve is due to sine flux distribution in the core. Following this, we have regions of

smooth declines where decay and deposition are happening in tandem. Regions with steep dips in the mass density correspond to rapid deposition – with the most deposition occurring across the heat exchanger enhanced by the small volume and large surface area (see Eq. 1) of this component.

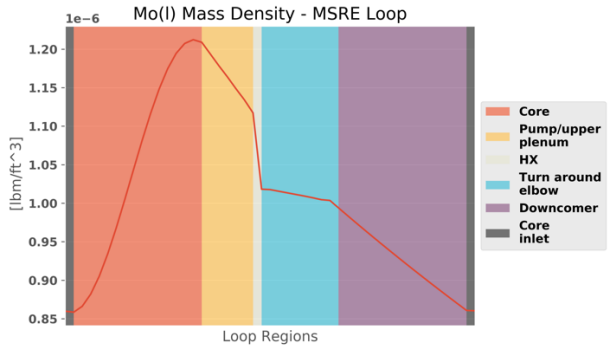

Figure 5. Mo(*l*) Mass Density.

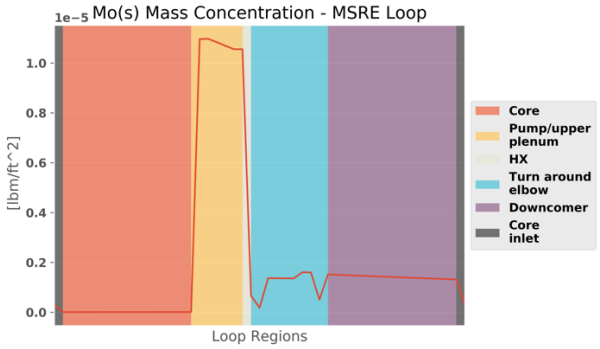

Figure 6. Mo(*s*) Mass Surface Concentration.

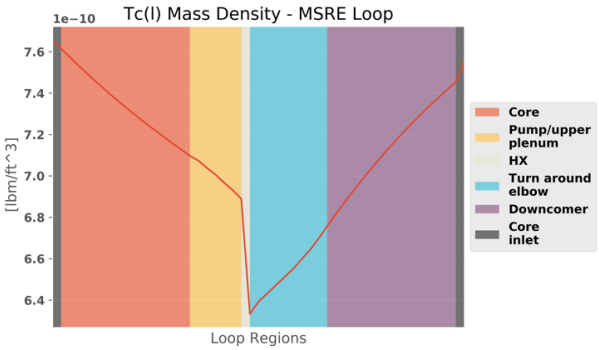

Figure 7. Tc(*l*) Mass Density.

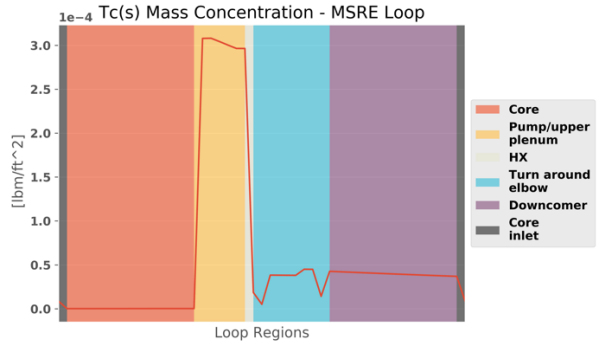

Figure 8. Tc(*s*) Mass Surface Concentration.

Tc(*l*) on the other hand behaves much differently as seen in Figure 7, with a decrease in the core via transmutation by the flux and larger neutron absorption cross section (25 barns). Following this, we have deposition occurring in the upper plenum and pump, with the largest deposition occurring once again in the heat exchanger. Since Tc(*l*) has a very long half-life (2e5 years), the loss due to decay is minimal, so the largest source term effects outside of the core are that of deposition and generation from Mo(*l*) decay which play against one another. Once the Tc(*l*) mass density has been sufficiently decreased via deposition in the heat exchanger, the generation through Mo(*l*) decay becomes greater than the diminished Tc(*l*) gradient driven deposition (see Eq. 1), so the species increases in the elbow and downcomer before it enters the flux region of the core where it once again experiences transmutation.

Looking next at the surface concentration species (*s*) in Figures 6 and 8, we see a uniform deposition profile which is a result of the fact that the mass transfer coefficients are species independent since the same diffusion coefficient used in the mass transfer coefficients is assumed for all NMs [3]. We also see these graphs are bumpy and have discontinuities due to the different surface areas of the geometric model and different mass totals in different parts of the loop. The largest surface concentration of NMs exist in the upper plenum and pump, which can be expected since the parent NM Mo(*l*) has the highest density, and thus the largest concentration driven gradient (see Eq. 1), at the outlet of the core. Once Mo(*l*) deposits in this region as Mo(*s*), subsequent Tc(*s*) will also build up here via decay and deposition from Tc(*l*).

Even though the highest surface concentration exists in the upper plenum and pump, that doesn't mean the majority of NMs are found here. This can be determined by looking at the mass totals for the ^{99}Mo – ^{99}Tc decay chain in the MSRE primary loop seen in Figures 9 – 10 below. Very quickly we see a large majority of the NMs deposit in the heat exchanger due to its large surface area (see Eq. 1) where the sharp discontinuity is due to the fact that the discretization in this region only has a single axial level within the channel. The large surface area is also why the surface concentrations seen in Figures 6 and 8 are so small in the heat exchanger, because even though the majority of metals are here, they are spread out over a large surface area. Also, we see a greater amount of Tc(*s*) deposited vs. Mo(*s*), since the only loss mechanism for a deposited species outside of the core is through decay into a different species and Tc(*s*) has a much longer half-life.

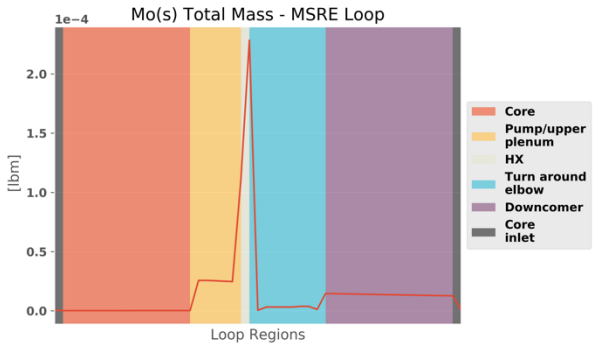

Figure 9. Mo(*s*) Total Mass.

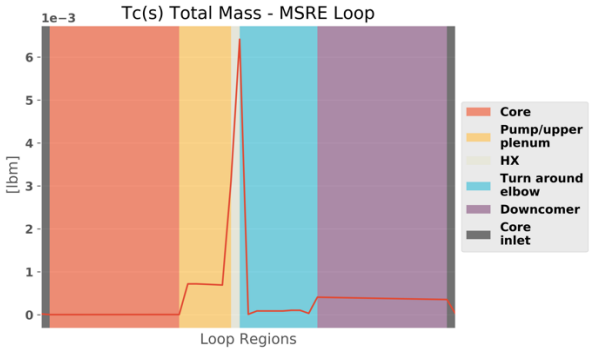

Figure 10. Tc(*s*) Total Mass.

The steady state solutions for the bulk fluid mass densities and mass surface concentrations for the ^{131}Sb – ^{131}Te – ^{131}Xe decay chain in the MSRE Simple Loop are presented below in Figures 11 – 14. As can be seen in the figures below, we see very similar results to the ^{99}Mo – ^{99}Tc decay chain with the small noted exception of Te(*l*) and I(*l*) concentration profiles seen in Figures 13 and 14. In this case, these bulk liquid species are not depositing in the reactor, but instead are receiving a source term from the deposited species Sb(*s*) and bulk species Sb(*l*). This can be seen clearly in that the largest source term for both Te(*l*) and I(*l*) is located in the heat exchanger, where a large amount of deposited Sb(*s*) is decaying back into soluble species rejoining the bulk flow.

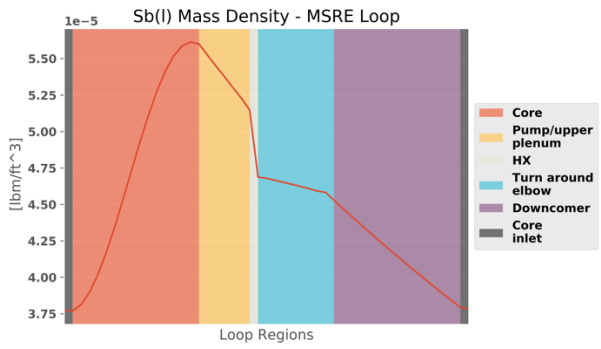

Figure 11. Sb(*l*) Mass Density.

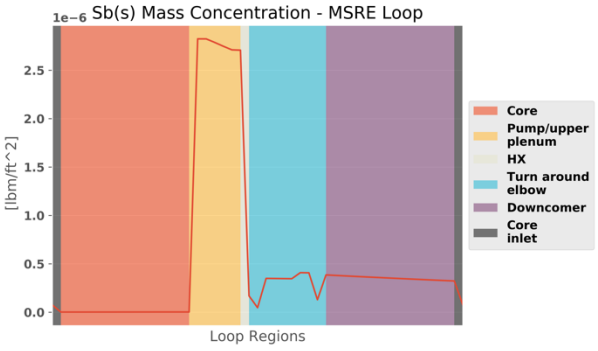

Figure 12. Sb(*s*) Mass Surface Concentration.

Both Te(*l*) and I(*l*) both experience transmutation in the core due to their larger neutron absorption cross sections (3 barns & 83 barns respectively). Te(*l*) has a short half-life (25 minutes) so its source term dependency is balanced between growth from Sb(*l*) and Sb(*s*) and decay into I(*l*). The majority of growth occurs in the upper plenum, pump, and heat exchanger regions since this is where large amounts of Sb(*s*)

is located. After this major growth, the Te(*l*) mass density decreases because the decay into I(*l*) is now dominant since Sb(*s*) and Sb(*l*) amounts are relatively smaller in the elbow and downcomer regions.

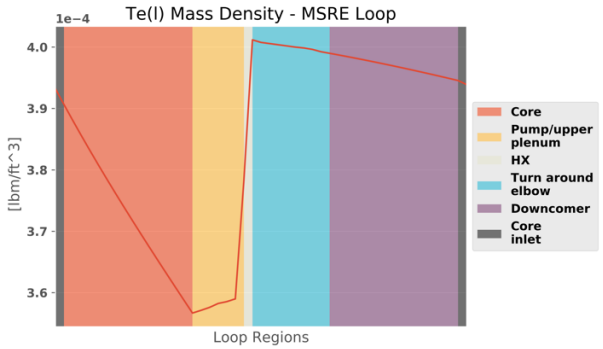

Figure 13. Te(*l*) Mass Density.

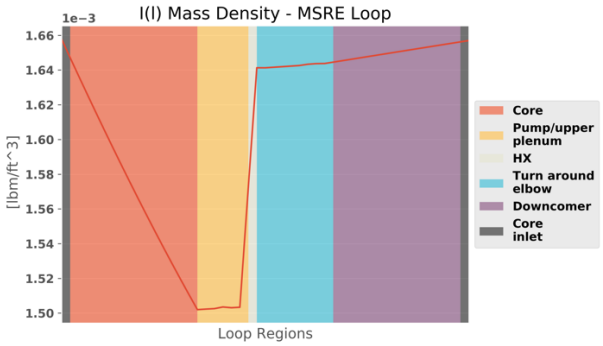

Figure 14. I(*l*) Mass Density.

I(*l*) growth is directly related to the behavior of Te(*l*) since Te(*l*) has such a short half-life. One thing to note however, is that I(*l*) has a much longer half-life (8 days), and as a result the only real loss for this species is through transmutation in the core. This is why the mass density increases in the elbow and downcomer – the growth from Te(*l*) decay is greater than the decay of I(*l*).

3.3. Comparison of Results with MSRE Experience

Lastly, we compared this data against the qualitative measurements of NM deposition during the MSRE ^{235}U and ^{233}U runs and the results are seen in below in Table 1 [3]. The NM CTF model performs reasonably well and captures the qualitative effect of NM deposition seen during the MSRE ^{235}U runs where there was negligible helium entrainment [3]. Since our model does not currently include any NM deposition to helium bubbles, this matches our models' assumptions of NM behavior during these runs. Current work is underway to implement NM deposition on helium bubbles which will enable us to model the MSRE ^{233}U runs where a significant amount of NM – bubble interactions occurred resulting in the large pump bowl accumulation of NMs [2][3].

Table I. Comparison of NM Deposition Model with MSRE Data

Region		HX	Metal Piping	Graphite	Pump – etc.
NM - CTF	% of NM	31.7%	52.5%	1.74%	14.0%
MSRE ^{235}U	% of NM	40.0%	50.0%	1.0%	9.0%
MSRE ^{233}U	% of NM	6.0%	8.0%	0.4%	86.0%

The largest source of error for the ^{235}U runs which skews our results is the discretization of our rudimentary MSRE model. It is quite apparent from the deposition results, that the upper plenum, pump, and heat exchanger regions are critical in NM deposition, and these regions need to be modeled with sufficient geometric surface area and volume resolution to capture the correct amount of deposition. Refining the geometric model should better balance the amount of NMs depositing on the heat exchanger versus the pump, and piping in this sensitive region.

4. DISCUSSION – FUTURE MSR DESIGN & EXPERIMENTAL NEEDS

Clearly, the NM deposition source/sink term is significantly large versus the other sink/source terms present in these decay chains and has a significant effect on the spatial dependence of the fuel salt composition. Additionally, the region directly at the outlet of the core is a sensitive region since there is a

generation of NMs in the core which rapidly plate out. If a NM filter will be installed in the loop, as some have envisioned, this is likely the best place for such a component. Ultimately, the placement of the heat exchanger, pump, and NM filter along with the thermal hydraulics of this region needs to be planned carefully since NM deposition can affect these components explicitly.

Additionally, in the event of a loss of coolant accident, this region of heavy NM deposition may require cooling to prevent structural damage, depending on the reactor size. It is also important to note that regions of high NM surface concentrations (in this case, the pump and upper plenum) will have greater concentrated decay heat, whereas regions like the heat exchanger will have a greater total amount of decay heat, but it will be smeared out over a much larger surface area.

The coupling of the thermodynamics code Thermochimica with CTF is currently underway which will allow the explicit determination of the fuel salt redox potential and resulting speciation of FPs in the fuel salt given the data for the FP species is available. If sufficient thermodynamic data for NM FPs can be simulated or measured, then the exact equilibrium concentration of NMs soluble in the fuel salt due to the temperature and redox potential can be determined, further refining the accuracy of this model. Some gibbs free energy of formation data points exist for metals in FLiBe, which can be used as a starting point for sensitivity analysis, but more data for NM species is needed [7].

5. FUTURE WORK

Ultimately, this work gives an initial capability for system wide analysis of NM deposition in a reactor primary loop. Future work will include mass transfer coefficient determination based upon the temperature, and flow conditions of the fuel-salt for predictive analysis specific to the geometric model. Additionally, work is currently underway to model NM deposition and transport via entrained bubbles; afterwards the effect of some chemical reactions/adhesion forces with the structural materials will be pursued. Finally, this NM mass transport model will be coupled with MPACT, the neutronics solver within VERA-CS, to see the overall multiphysics effect that NM mass transport has on reactor dynamics and long-term behavior due to fuel-salt composition changes and decay heat generation.

ACKNOWLEDGMENTS

This material is based upon work supported under an Integrated University Program Graduate Fellowship.

REFERENCES

1. E.L. Compere et al, “Fission Product Behavior in the Molten Salt Reactor Experiment,” ORNL-4865, Oak Ridge National Laboratory (1975).
2. J. Engel et al, “Spray, Mist, Bubbles, and Foam in The Molten Salt Reactor Experiment,” ORNL-TM-3027, Oak Ridge National Laboratory (1970).
3. R. J. Kedl, “The Migration of a Class of Fission Products (Noble Metals) in the Molten-Salt Reactor Experiment,” ORNL-TM-3884, Oak Ridge National Laboratory (1972).
4. R. S. Tanaka, “Quantifying the Adhesion of Noble Metal Foulants on Structural Materials in a Molten Salt Reactor,” MS Thesis, MIT, Nuclear Science and Engineering (February 2017).
5. Z. Taylor, R. Salko, B. Collins, “Implementation of General Species Transport Capability into VERA-CS for Molten Salt Reactor Analysis,” Trans. Am. Soc., **118**, 1061-1064 (2018)
6. J. L. Plawsky, *Transport Phenomena Fundamentals*, 3rd ed, 121-127, Taylor & Francis Group (2014).
7. M. Sohal, M. Ebner, P. Sabharwall, P. Sharpe “Engineering Database of Liquid Salt Thermophysical and Thermochemical Properties,” INL/EXT-10-18297, Idaho National Laboratory (2010).